



HARD CLUSTERING OF ESN DYNAMICS USING CONCEPTORS

Bachelor's Project Thesis

Joris Peters, s4001109, j.peters.13@student.rug.nl,

Supervisors: G.Pourcel & Prof Dr H. Jaeger

Abstract: For data analysis, explainability, and neuro-symbolic integration, it can be of interest to identify groups and hierarchies within the activity dynamics of recurrent neural networks (RNNs). Using conceptors to represent RNN dynamics, this study aims to cluster the dynamics of Echo State Networks (ESNs), a variant of RNNs. Conceptors were computed from the ESN-response to phoneme recordings of the TIMIT dataset. These conceptors were then used to perform phoneme classification (supervised), clustering with an adaptation of K-means (unsupervised), and hierarchical clustering with average linkage (partly supervised). Conceptor-based phoneme classification reached a reasonable accuracy. Moreover, I show that conceptors may be used for clustering neural ESN activities into distinct groups and hierarchies that resemble existing phonetical taxonomies. I conclude that conceptors are well-suited to classifying and clustering ESN-dynamics and the time-series that induced these dynamics.

Dear reviewers,

In this project, I aim to identify relevant clusters within the dynamics of Echo State Networks. The version you are reading is not final. Some of what I will still add I noted between [square brackets]. **[Bold parts]** are open questions, some of which are in response to (Guillaume's) earlier comments. The methods and results reached a state, where I think feedback would be very useful. However, after recently changing the narrative again, I was unable to render the introduction and discussion coherent, and had to leave them mostly out for this submission, since they would have been more a source of confusion than subject to constructive feedback. Nonetheless, you can find a collection of the ideas that I currently writing together in the additional "draft.docx" document.

To give you some form of explanation for the slow progress, it is largely due to my psychological instability, still ongoing because of being related to this project and how I (my mind) interprets it. I have several fears and it is my responsibility to face them. I am thankful for your patience and any feedback that you may be able to give. I am committed to finishing in September.

Best, Joris

1 Introduction

1.1 Background

[Paragraph: Representations, definitions:] The study of *representations* is key to understanding and developing neural networks. Neural networks like the human brain or artificial neural networks (ANNs) represent contents and process these representations to exhibit useful behavior (Kriegeskorte and Kievit, 2013). The *representational contents* could range from concrete sensory inputs like sounds or images to abstract concepts like "I" or "robot". The *representations*, likewise depending on the model, could range from localist representations as single neurons (grandmother neuron) to connectionist representations as patterns of neuronal firing of a network of neurons. Computationalists model cognition like reasoning, creativity, memory, and language as processes on neurally represented contents. For example, speech classification can be seen as linking an input utterance to the class representation. Moreover, cognitive performance can strongly vary in function of the underlying representation as seen in chunking tasks [(Miller, 1956), (Chase and Simon, 1973)]. For an integrated understanding of neural networks and cognition and to develop and explain artificial neu-

ral networks, tools for the study of representations are needed.

[Paragraph: Study of stimuli representations] Cognitive neuroscience has long studied the nature of neural representations in the brain. These studies commonly distinguish three types of spaces in the context of some neural network (a brain region, a population of neurons, etc) and representational content. First, input spaces contain sets of relevant inputs to the network. For example, an input space may span the possible speech utterances of a certain length and dimensionality. Stimulus, sensory, emotional, physical, color, and even representational spaces can be seen as instances or nuances of input spaces. Second, representational spaces contain the possible neural states or state sequences in a neural network. Third, semantic spaces contain the possible "meanings" that arise in a system (a discussion on the substrates of meaning is beyond the scope).

[Paragraph: Representational geometries, and clustering methods for analyzing representational geometries]

[Paragraph: The nature of the representation; spiking patterns, and symbols]

[Paragraph: Representations of symbols in the brain, Speech/phonemic data, TIMIT dataset, representational geometry study on TIMIT]

[Paragraph: Study of stimuli representations in AI, XAI (without conceptors)]

[Paragraph: Study of representation of symbols in AI (using conceptors)]

[Paragraph: Motivation]

[Paragraph: What is unknown?]

[Paragraph: RQ] How to identify distinct and meaningful clusters within the an RNN's representation of stimuli?

[Paragraph: Proposed Solution]

[Paragraph: Additional motivations]

[Paragraph: Study limitations]

[Paragraph: Key Insights / Findings]

1.1.1 Structure

The next section provides formal definitions and an intuition of ESNs and conceptors. The methods section begin with a description of the data, its pre-processing, and the collection of ESN state representations of the data. Experiment 1 is a phoneme classification task used to tune the ESN to the data and demonstrate the efficacy of conceptor-based

methods. In Experiment 2, the ESN's representation of individual stimuli (phonemic utterances) will be clustered. Experiment 3 will attempt to distill hierarchies from the ESN's representations of symbols (phonemes). The results are mentioned after the methods of the respective experiments. Finally, all results will be discussed and an outlook application and future developments of the methods in the context of speech-processing, XAI, and neuro-symbolic AI will be provided.

1.2 Formal Definitions

The following sections on ESNs and conceptors were inspired by the detailed report Jaeger (2014). Appendix B contains an index of mathematical notations used throughout the paper.

1.2.1 Echo State Networks

Let us formalize an example ESN like the one from Figure ?? . Let N be the number of internal neurons. As mentioned, N will typically be large relative to the dimensionality d of the input. The input weight matrix $W^{in} \in \mathbb{R}^{N \times d}$, the bias vector $b \in \mathbb{R}^N$, and the internal weight matrix $W \in \mathbb{R}^{N \times N}$ are randomly initialized, the latter of which will typically contain many zeros to implement the internal sparsity of the reservoir. When driven by a discrete time series input u of length L , the ESN elicits a response, the internal state sequence x of dimensionality N and of the same length as the input. The ESN's update equation is that of classical discrete-time RNNs:

$$x(n+1) = \tanh(Wx(n) + W^{in}u(n+1) + b), \quad (1.1)$$

where $x(n)$ and $u(n)$ are the internal reservoir state and input column vectors at time step n and \tanh is the hyperbolic tangent. Observe that any ESN state depends on the current input and the ESN's previous internal state. Indeed, the response x is a high-dimensional non-linear expansion of the input since $N \gg d$ and \tanh is applied. For later convenience, I define function r from the set of input sequences to the set of response sequences where $r(u)$ is the response that results from driving the ESN with u . The used ESN and the parameters will be clear from the context where r is used.

1.2.2 Conceptors

Definition and Intuition Given any sequence of network states $x = (x(1), \dots, x(L))$ that may have arisen from running the above ESN *, the conceptor matrix C computed from x minimizes the following loss function \mathcal{L} :

$$\mathcal{L}(C|x, \alpha) = \sum_{n=1}^L \|x(n) - Cx(n)\|^2 / L + \alpha^{-2} \|C\|^2$$

$$C = \arg \min_C \mathcal{L}(C|x, \alpha), \quad (1.2)$$

where $\alpha \geq 0$ is the conceptor's aperture (further explained below). The conceptor C that minimizes $\mathcal{L}(C|x, \alpha)$ may be analytically computed via the following procedure:

1. Concatenate the states in x column-wise in an $N \times L$ collection matrix $X = [x(1)|\dots|x(L)]$.
2. Compute the correlation matrix $R = XX'/N \approx \text{corr}(X)$.
3. Obtain the conceptor $C(R, \alpha) = R(R + \alpha^{-2}I)^{-1}$ with $N \times N$ identity matrix I .

To provide some intuition, conceptors can be considered "fingerprint" of the activity of [a] network" over a period of time (Jaeger, 2014). This potential for conceptors to uniquely identify or fingerprint a sequence of states is reflected in its loss function. When minimizing \mathcal{L} , the term $\|x(n) - Cx(n)\|^2$ nudges C toward realizing an identity mapping for the states $x(n)$. However, the regularization term $\alpha^{-2}\|C\|^2$ attaches a cost to the magnitude of its entries, limiting the numerical resources available to realize this identity mapping. Thus, the conceptor is drawn away from the identity matrix toward the zero matrix, especially on those axes that can account for little of the variance of x , i.e., where the minimization of $\|x(n) - Cx(n)\|^2$ is less beneficial. The amount of regularization applied to the conceptor depends on its aperture α . The higher the aperture, the closer the resulting conceptor maps all the members of x to themselves. The lower the

aperture, the more selective the conceptor becomes, realizing a "good" identity mapping only along the important axes that explain most of the sequence's variance.

A geometric perspective might extend this intuition. The reservoir states being a point cloud in state space $(0, 1)^N$, their conceptor can be represented as a hyperellipsoid of a similar shape as the point cloud but constrained to the unit circle of \mathbb{R}^N . The directions and lengths of the hyperellipsoid's axes are given by the singular vectors and values of the conceptor, respectively, and "represent the principle components of the state cloud" (Vlegels, 2022). However, the shape of the hyperellipsoid slightly deviates from that of the point cloud as the regularization *squashes* it along its shorter axes. With a low aperture, the hyperellipsoid would be very squashed, extended only along a few main axes. With a large aperture, the conceptor would be a little squashed and approach the unit hypersphere.

This squashing in space may be seen as a spatial compression as it systematically reduces the variance of the point cloud along its less important axes. Furthermore, conceptors are a temporal compression of ESN state sequences. Mapping sequences of vectors in state-space to conceptor-space turns variable-length objects into constant-sized objects. When the state sequence is a time series, this mapping removes the temporal dimension, whence it may be seen as a temporal compression. **[Is there a better way to describe this compression?]**

Conceptor operations The following section describes several useful operations on conceptors some of which illustrate their symbolic nature. [Elaborate]

Similarity function Conceptors may be used to compute the similarities of state sequences. If C_a and C_b be the conceptors derived from the two sequences of states to be compared, their similarity may be defined as:

$$\text{Sim}(C_a, C_b) = \frac{|(S_a)^{1/2}(U_a)'(U_b)(S_b)^{1/2}|^2}{|\text{diag}(S_a)||\text{diag}(S_b)|}, \quad (1.3)$$

where $U_a S_a (U_a)'$ is the SVD of C_a and $U_b S_b (U_b)'$ is the SVD of C_b . It is a function of the squared cosine similarity of the conceptors that measures the angular alignment between all pairings of singu-

*I consider *sequences* of network states for practicality, but they can be thought of as *sets* because their states need not necessarily be ordered; any ordinal information is lost during the computation of conceptors. Neither do the states need necessarily stem from the same ESN run.

lar vectors of the two conceptors weighted by the corresponding singular values.

Aperture The aperture of a conceptor can be set during its computation or when given a pre-computed conceptor C [Is it okay to use the name 'C' to refer to other conceptors than this one. Or do I need to name every object differently e.g., C_2 .], its aperture can still be adapted by any factor of $\gamma > 0$ using the aperture-adaptation function φ that returns the aperture-adapted conceptor C_{new} :

$$C_{new} = \varphi(C, \gamma) = C(C + \gamma^{-2}(I - C))^{-1} \quad (1.4)$$

Logical Operations on Conceptors Several logical operations have been meaningfully defined on conceptors. Given two conceptors C and B , we have the following definitions and semantics:

1. **Negation** (\neg)

$$\neg C := I - C \quad (1.5)$$

It returns a conceptor that describes the linear subspace complementary to that of C .

2. **Conjunction** (\wedge)

$$C \wedge B := (P_{R(C) \cap R(B)}(C^\dagger + B^\dagger - I)P_{R(C) \cap R(B)})^\dagger \quad (1.6)$$

See Appendix A.1 for details on the computation of $P_{R(C) \cap R(B)}$. It returns a conceptor that describes the intersection of the linear subspaces of C and B .

3. **Disjunction** (\vee)

$$C \vee B := \neg(\neg C \wedge \neg B), \quad (1.7)$$

by De Morgan's law. It returns a conceptor that describes the union of the linear subspaces of C and B .

Although a simpler method for computing conjunction and disjunction exists, that method relies on the inversion of B and C and thus fails when B or C contain singular values of 0. Such singular values may occur in practice, for example, due to rounding or through the negation of conceptors with unit singular values. Therefore, the above method is recommended whenever the absence of null and unit singular values cannot be ensured.

2 Methods and Results

2.1 Dataset

The TIMIT Acoustic-Phonetic Continuous Speech Corpus (TIMIT) was chosen as the data source, for it features diverse and phonetically annotated speech signals. TIMIT comprises 6300 sentence utterances. Each of the 630 US-based native-English speakers (from eight dialect regions and 30% of whom were female) read ten sentences: five phonetically-compact, three phonetically-diverse, and two dialect sentences. Each utterance comes with a phonetic transcription that indicates which of 64 phones is uttered at any time. Moreover, the corpus is pre-split into a training (73 % of the utterances) and a test set used as such in Experiment 1. Experiments 2 and 3 relied solely on the training set.

2.2 Pre-processing

For all experiments, the following pre-processing steps were performed. The utterances were segmented according to the phonetic transcriptions into $n = 241225$ segments ($n_{\text{TIMIT-train}} = 177080$ and $n_{\text{TIMIT-test}} = 64145$), each a vocalization of one phone (Figure 2.1). From each segment, the first $d = 13$ Mel Frequency Cepstral Coefficients (MFCCs) were extracted, consistent with previous literature Bromberg, Qian, Hou, Li, Ma, Matthews, Moreno-Daniel, Morris, Siniscalchi, Tsao, et al. (2007). This representation ought to isolate the information most relevant to speech analysis. To compute the MFCCs, the Librosa Python library (McFee, Raffel, Liang, Ellis, Mcvcar, Battenberg, and Nieto, 2015) was used with one MFCC vector computed every 1 ms from a 2.5 ms long sliding window.

The resulting time series were normalized in amplitude and time. First, the amplitudes varied strongly across the channels [the lowest mean amplitude of an MFCC channel ($\mu_1 = -593.2$) is 24.2 times lower than that of the second lowest channel ($\mu_4 = -22.4$)]. To grant each MFCC a similarly strong effect on the ESN dynamics under the identically distributed input weights, each channel was normalized to a range of $[-0.5, 0.5]$ across all samples. Second, to account for differences in utterance speeds, the series were normalized in time by fitting each channel with a cubic spline and sampling it at

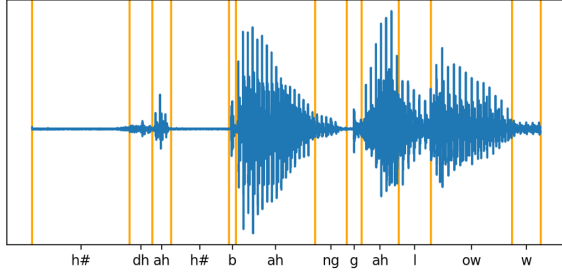


Figure 2.1: Example of the twelve first segments of one of the utterances.

$L = 10$ temporally equidistant points.

Lastly, the phonetic labels (transcriptions) p_i ($i = 1, \dots, c$) were mapped from the original set of 61 phones to a subset of 39 phonemes P . Initially proposed by Lee and Hon (1989), this mapping (Table A.1) amounts to folding stress-related variations and allophonic variations of phonemes (e.g., /em/ and /m/) into the same classes. This was done to reach reasonable classification and clustering performances, feasible computations, and results comparable to previous studies that also used the mapping [add citations].

Thus, the resulting data consisted of tuples $D = \{(s_i, p_i) | i = 1, \dots, c\}$ with MFCC time series s_i , phone labels $p_i \in P$, and the set of phones P after folding ($|P| = 39$). The ready-made train-test split from TIMIT was used giving $D_{\text{TIMIT-train}}$ and $D_{\text{TIMIT-test}}$ of respective lengths $n_{\text{TIMIT-train}}$ and $n_{\text{TIMIT-test}}$.

2.3 ESN

The following ESN setup was used for all three experiments. Its hyperparameters are summarized in Table 2.1. The ESN consisted of $N = 100$ neurons with a connection density of $r = 10\%$. The entries of W^{in} and b were randomly sampled from a standard normal distribution and rescaled by factors of $k_{W^{in}} = 1.0$ and $k_b = 0.6$, respectively. W was obtained by random sampling from a standard normal distribution and rescaling the result to a spectral radius of $\rho = 2.3$. The spectral radius of an internal weight matrix is its largest absolute eigenvalue. The larger ρ , the farther W transforms the internal state during the state update along its first eigenvector, which tends to lead to a more chaotic behavior. ρ

was adapted by rescaling the old (initial) internal weight matrix W_{old} to $W_{new} = \frac{\rho_{new}}{\rho(W_{old})} W_{old}$ where W_{new} has the desired spectral radius ρ_{new} instead of the previous ρ_{old} . [Effects on ESP]

Hyperparameter	Value
Number of neurons (N)	100
Connection density (r)	10%
Scaling factor for W^{in} ($k_{W^{in}}$)	1.0
Scaling factor for b (k_b)	0.6
Spectral radius (ρ)	2.3

Table 2.1: Final ESN hyperparameters.

The above hyperparameters were picked by hand based on their effects on the accuracy in Experiment 1, previous research, and resource constraints. All parameters were initially set to the values used in the demonstration experiments of (Jaeger, 2014) (Section 4.1, p. 161). N was kept as a largest possible value still feasible under the available computational resources. Larger sizes would likely improve performance after adapting the other hyperparameters but may increase the risk for overfitting (Lukoševičius, 2012). The remaining hyperparameters, r , $k_{W^{in}}$, k_b , and ρ , were adjusted by hand with the objective to maximize the development accuracy of phoneme classification in Experiment 1 [Is this a sufficient explanation of the picking process? Or would a grid-search be necessary (I performed it informally)?]. Moreover, automated hyperparameters optimization was attempted but eventually not used due to its large computational cost and slow convergence that made waiting for its convergence intractable. Its method and results are in the Appendix.

The resulting ESN was driven independently on each input signal s_i ($i = 1, \dots, c$) producing the reservoir state sequence x_i ($i = 1, \dots, c$). Concretely, each run started from the same state $x(0)$ sampled once from a standard normal distribution not to introduce meaningless between-sample differences while providing the network with an initial excitation. Indeed, using this normally distributed starting state led to a greater classification accuracy ([add correct value] ... on D_{dev} using the final hyperparameters) in Experiment 1 than when using the null vector as the starting state [Can/Should I just state this without reporting the experiment? And is it tolerated to make such design decisions

using the test set given the risk of overfitting?]. The following states $x_i(t)$ ($t = 1, \dots, L$) were computed via update Equation 1.1 and collected column-wise in $N \times L$ matrix $X_i = [x_i(1)|\dots|x_i(L)]$. Concluding, an ESN response collection matrix X_i was computed for each training sample.

2.4 Experiment 1: Phoneme Classification

[For this experiment 1’s lengthiness, I suspect some parts might be better placed in the appendix (?)] **Objective** Experiment 1 aimed to classify the pre-processed utterances using the corresponding ESN responses. The experiment’s purpose is to (a) optimize the ESN hyperparameters for the subsequent clustering experiments and (b) evaluate and improve methods for conceceptor-based time series classification. Concretely, the developed classifier takes as input the ESN’s response to an utterance and outputs the assigned phoneme label. The assigned label is taken to equally apply to the ESN’s response to the utterance and the utterance.

Data To optimize hyperparameters and take small design decisions, the pre-processed original dataset $D_{\text{TIMIT-train}}$ was initially divided into a preliminary training set, $D_{\text{pre-train}}$, and a development set, D_{dev} . Here, the split was 80/20, respectively, stratifying over phonemic classes. Once hyperparameters and methods were set, the classifier was retrained on the whole of $D_{\text{TIMIT-train}}$ and evaluated on $D_{\text{TIMIT-test}}$.

2.4.1 Training

Training amounted to computing one *positive conceceptor* C_p^+ and one *negative conceceptor* C_p^- per class $p \in P$. Each class’ positive conceceptor captures the linear state subspace that ESN states (responses to pre-processed phoneme utterances) of that class tend to occupy. For each class p , it was computed as follows. Let η_p be the number of training instances of p . The state collection matrices corresponding to signals of p were concatenated column-wise into a class-level collection matrix $X_p = [X_1|X_2|\dots|X_{\eta_p}]$ from which C_p^+ was computed with an initial aperture of $\alpha = 1$ by steps 2 and 3 of the procedure for conceceptor computation. This was repeated for each class to obtain the set of preliminary positive conceptors $C_{pre}^+ = \{C_p^+ | p \in P\}$.

Aperture adaptation After computing the conceptors in C_{pre}^+ with the initial aperture of $\alpha = 1$, their apertures were optimized. First, one new aperture α_{opt} was chosen for all positive conceptors. The objective was to maximize their sensitivity to differences in the underlying ESN dynamics which would likely improve their capacity to classify the data to come. This objective is quantified as the maximization of the ∇ -*criterion*. Concretely, the ∇ -*criterion* is defined in function of conceceptor C and a candidate aperture adaptation factor γ [†]. It then returns the gradient of the Frobenius norm of the aperture-adapted conceceptor with respect to the logarithm of γ :

$$\nabla(C, \gamma) = \frac{d}{d \log(\gamma)} \|\varphi(C, \gamma)\|^2 \quad (2.1)$$

Indeed, this corresponds to the magnitude at which the size $\|C\|^2$ of a conceceptor C changes (sensitivity) with respect to its log aperture (scaling of the underlying ESN states, see p. 49 of Jaeger (2014)). The optimal aperture, γ_p , was then approximated for each positive conceceptor C_p^+ by sweeping through 200 candidate values $\gamma_{candidate}$ in the interval $[0.001, 500]$ on a logarithmic scale; logarithmic, for the optimal value was expected on the lower end of the interval. γ_p was set to the $\gamma_{candidate}$ that maximized a numerical approximation of $\nabla(C_p^+, \gamma_{candidate})$. This derivative was approximated using a change in γ of $\Delta\gamma = 10^{-4}$ [Does the method for approximating the derivative need further explanation?]. $|P| = 39$ values γ_p ($p \in P$) resulted. Finally, the apertures of all positive conceptors were adapted using the mean $\gamma_{opt} = \frac{1}{|P|} \sum_{p \in P} \gamma_p \approx 133.98$. Let C_{opt}^+ be the resulting set of aperture-optimized positive conceptors.

The reason for adapting all conceptors to the same aperture instead of adapting each conceceptor with their γ_p is to avoid classification bias. The larger a conceceptor’s trace (the sum of its singular values), the larger its *expected* Evidence, the similarity measure later used for classifying new instances [Should I add the proof to appendix?]. Thus, if there are differences between the traces of the conceptors, the classifier will be biased toward the classes whose conceptors have greater traces. A similar bias occurs for the expected conceceptor similarity

[†]In this case, γ equals the resulting aperture α_{new} , since $\gamma = \frac{\alpha_{new}}{\alpha}$ and the current aperture $\alpha = 1$.

later used for clustering. Since a conceceptor's trace strongly covaries with its aperture, the latter is used to control the trace [Do I need a citation, proof, or explanation for this?]. Thus, equating the apertures between classes helped as first step to approach their traces and debias the classifier.

However, although the conceceptors were adapted to the same aperture, some variation in their traces remained as can be seen at $x = 1$ in Figure 2.2. To remove it, the conceceptor's traces were again adapted until reaching a shared target value $tr_{target} = \bar{tr}$, the mean trace among the conceceptors:

$$\bar{tr} = \frac{1}{|C^+|} \sum_{C \in C_{opt}^+} tr(C) \approx 57.23 \quad (2.2)$$

To adapt each conceceptor's trace to this target value with an error tolerance of ϵ (here, $\epsilon = 0.01$), Algorithm 2.1 was developed. I shall call $\psi(C, tr_{target}, \epsilon)$ the function computed by the algorithm. The iterative procedure adapts a conceceptor's aperture by a factor of the current trace error ratio until reaching the target trace. This works because, again, trace and aperture covary.

Algorithm 2.1 Adapt the trace of a conceceptor

Require:

Conceceptor C whose trace is to be adapted to tr_{target}
 Target trace tr_{target}
 Error tolerance ϵ

while TRUE **do**

if $|tr_{target} - tr(C)| < \epsilon$ **then**
 break

end if

$\gamma \leftarrow tr/tr(C)$

$C \leftarrow \varphi(C, \gamma)$

end while

As shown in Figure 2.2 at $x > 1$, applying $\psi(\cdot, \bar{tr}, 0.01)$ to each of the conceceptors in C_{opt}^+ normalizes their traces. Thus, via the above two aperture adaptation procedures, the apertures of the conceceptors in C_{pre}^+ were optimized and their traces were normalized resulting in the final set of positive conceceptors C^+ .

Negative conceceptors From C^+ , the set of negative conceceptors $C^- = \{C_p^- | p \in P\}$ was computed.

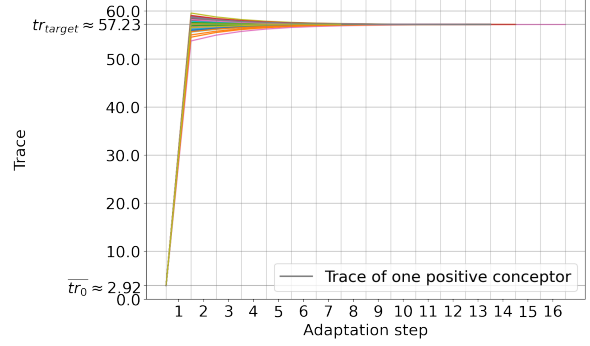


Figure 2.2: The traces of the positive conceceptors in function of the adaption steps. The first adaptation step 1 is the aperture adaptation based on the ∇ -criterion. The increase in aperture caused the traces to increase and diverge. The remaining steps ($x > 1$) are the results of normalizing the traces using Algorithm 2.1. Finally, these aperture adaptation steps resulted in an increase of the mean trace from an initial value of \bar{tr}_0 to approximately the target value tr_{target} .

Each class' negative conceceptor models the linear state subspace that is complementary to the space occupied the states of all other classes. Or, equivalently, it models the subspace that states "from none of the other classes" are expected to occupy. These semantics are reflected in their formal definition:

$$C_p^- = \neg \bigvee \{C_q^+ | q \in P, q \neq p\}, \quad (2.3)$$

where $\bigvee S$ is the disjunction of the $|S|$ conceceptors in set S computed by the associative disjunction of its elements:

$$\bigvee S = ((C_1 \vee C_2) \vee C_3) \vee \dots \vee C_{|S|} \quad (2.4)$$

Adapting the apertures of the resulting C_p^- , using the methods with which the positive conceceptors were adapted, did not improve the development accuracy.

2.4.2 Testing

The combined Evidence E was used to classify unforeseen speech samples via the corresponding ESN responses. The combined Evidence $E(x, p)$ that some ESN state x corresponds to class p is a measure of similarity between that state and the positive and negative conceceptors of class p . Concretely, it

is the combination of a positive Evidence $E^+(x, p)$, computed using the positive concepthor C_p^+ , and a negative Evidence $E^-(x, p)$, computed using the negative concepthor C_p^- :

$$\begin{aligned} E(x, p) &= E^+(x, p) + E^-(x, p), \\ E^+(x, p) &= x' C_p^+ x \\ E^-(x, p) &= x' C_p^- x \end{aligned} \quad (2.5)$$

$E(x, p)$ is large when x is close to the linear subspace modeled by concepthor C_p^+ , but far from the linear subspace which the other concepthors model (see definition of C_p^-).

To classify a state x , the positive Evidence is maximized over all classes:

$$\text{Class}'(x) = \arg \max_{p \in P} E(x, p) \quad (2.6)$$

[Can I use self-explanatory symbols like **Class'** without explicitly stating what they are.] To classify a point cloud X (a column-wise state collection matrix), the mean Evidence for all states (columns of the collection matrix) is taken:

$$\text{Class}(X) = \arg \max_{p \in P} \frac{1}{L} \sum_{i=1}^L E(X[:, i], p), \quad (2.7)$$

where L is the width of X .

Finally, given a speech sample s_{new} , $\text{Class}(X_{new})$ returns the classification estimate, where $X_{new} = [r(s_{new})(1) \dots r(s_{new})(L)]$ is the column-wise concatenation of the states collected when driving the ESN with s_{new} (excluding the starting state).

2.4.3 Results

Table 2.2 shows the resulting accuracies. For additional reference, the confusion matrix in Figure A.1 of Appendix A shows the classification rates across the classes. In an attempt to improve the accuracy, the experiment was repeated in slight adaptation to the type of data (Appendix A) which led to a training accuracy of 63.64% but test accuracy of 49.13%.

Transition In Experiment 1, an ESN setup (see Table 2.1) was found that could effectively represent time series as reflected in the accuracy achieved during concepthor-based classification. The same ESN

Domain	Accuracy (%)
Development	55.66
Train	53.82
Test	53.83

Table 2.2: Development, training, and test accuracies.

setup and similar concepthor-based mechanisms were reused in Experiments 2 and 3 as I turn to unsupervised methods for identifying distinct symbols within ESN dynamics.

2.5 Experiment 2: Below-phoneme clustering

Objective Now blinded of any a-priori groups – the classes $|P|$ previously available during training – the unlabeled ESN responses to the MFCC time-series (pre-processed phoneme utterances) were clustered. Concretely, in Experiment 2 had three conditions for grouping the earlier computed ESN state clouds into K hard (non-overlapping) clusters and one baseline condition, where the corresponding MFCC time-series were clustered.

Dataset For computational constraints, the experiment was run on data subsamples $D_l \subset D_{\text{TIMIT-train}}$ but was repeated 10 times ($l = 1, \dots, 10$). Each D_l encompassed utterances of an *independently* sampled set of 7 phonemes P_l to reduce selection bias. The cardinality of $|P_l| = 7$ ought roughly align the difficulty of the current task with the "simple" condition of a previous study, (Lerato and Niesler, 2012), that similarly performed hard clustering on TIMIT's phoneme recordings. However, since (Lerato and Niesler, 2012) restricted the data to vowels, which I did not for consistency with Experiment 3, their task was likely more difficult. For each phoneme in P_l , 15 phoneme utterances were sampled, to meet the centroid-based clustering assumption of equally large clusters, for a total of $n' = 105$ utterances per subset. Concretely, each utterance was sampled from 48 random speakers with an equal ratio across genders and dialect regions (newly sampled for each fold l). This stratification aims to evenly represent the population and enable the evaluation of any found clusters on and their generalization to new data. Moreover, only

utterances from the phonetically compact sentences, that use each phonemes in a few phonetic contexts (e.g., /aa/ only before /f/), were considered to limit phonetic variability.

Clustering Scheme On each D_l , generalized centroid-based clustering was performed in four conditions. I will proceed by describing the algorithm, that is parameterized by three condition-dependent components, and then elaborate on the conditions. Besides the desired number of clusters K , the generalized centroid-based clustering algorithm is parametrized by three components:

1. A set of points $D = \{p_1, p_2, \dots, p_n\}$ to be clustered.
2. A centroid computation function $\text{centroid}(Cl)$ that provides the centroid of a given cluster Cl (a set of points).
3. A dissimilarity function $d(p_i, \mu_j)$ that provides the dissimilarity of a point p_i and centroid μ_j . During the assignment step, points are assigned to the cluster with the most similar centroid. This function is assumed to be non-negative and be monotonic increasing with dissimilarity. It may be asymmetric.

The algorithm minimizes the following loss function L :

$$L = \sum_{k=1}^K \sum_{p_i \in Cl_k} d(p_i, \text{centroid}(Cl_k)), \quad (2.8)$$

where Cl_k is the set of points in the k^{th} cluster.

L is minimized by as follows. Centroids are initialized in a K-means++ fashion. With this method, the initial centroids are sampled from a distribution that aims to spread them evenly across point space. Compared to the random centroid-initialization of classical K-means, this method tends to converge faster and more consistently used on points in Euclidian space (Arthur and Vassilvitskii, 2007). Then, two steps are iteratively repeated. In the *Assignment step*, each data point is assigned to the cluster with the nearest centroid according to some distance function. In the *Centroid update step*, the centroids are recalculated based on the newly formed clusters. This process terminates once all centroids converged

Algorithm 2.2 Generalized centroid-based hard clustering algorithm

Require:

- Number of clusters K
- [1] Set of points $D = \{p_1, p_2, \dots, p_n\}$
- [2] Centroid computation function $\text{centroid}(Cl)$
- [3] Dissimilarity function $d(p_i, p_j)$

Initialize K cluster centroids via the K-means++ procedure: $\mu = \{\mu_1, \mu_2, \dots, \mu_K\}$

while TRUE **do**

Reset all clusters: $Cl = \{\emptyset, \emptyset, \dots, \emptyset\}$

Assignment step:

for p_i in D **do**

$k \leftarrow \arg \min_{1 \leq j \leq K} d(p_i, \mu_j)$

Assign p_i to cluster k : $Cl_k \leftarrow Cl_k \cup p_i$

end for

Reassignment step for empty clusters:

while any Cl_j is empty **do**

Find point p_{max} in D that is most dissimilar to the centroid of its current cluster

Move p_{max} from its old cluster to Cl_j^\dagger

end while

Centroid update step:

for $j = 1$ to K **do**

$\mu_j \leftarrow \text{centroid}(Cl_j)$

end for

if cluster assignments did not change **then**

break because converged

end if

end while

return Set of clusters $Cl =$

Cl_1, Cl_2, \dots, Cl_K

in their position or a maximum number of iterations is reached.

Empty clusters were actively prevented. It is theoretically possible for empty clusters to arise after the *Assignment step* in each condition. An explanation will be given in the discussion. In practice, this case only occurred in the conceptor-based conditions (*ESN-Evidence* and *ESN-Mixed*). Regardless, since no decent centroid can be found for empty clusters, this case was handled in an additional *Reassignment step* after the *Assignment step*. Concretely, when an empty cluster arises, the most "misfit" point – the point with the largest dissimilarity to its current cluster's centroid – is reassigned to the empty cluster.

Conditions The experiment was performed in four conditions that would determine the parameters of the generalized centroid-based clustering algorithm:

- *MFCC-Euclidian* was a baseline where the MFCC time series were clustered using classical K-means(++).
- *ESN-Euclidian*, *ESN-Evidence*, and *ESN-Hybrid* clustered ESN state clouds, the responses to the MFCC time series.

First, in the *MFCC-Euclidian* condition, classical K-means was used to cluster the MFCC time series directly.

1. The set of points $D_{MFCC,l}$ contains the unlabeled MFCC time series D_l :

$$D_{MFCC,l} = D_l = \{s_i | 0 < i \leq n'\} \quad (2.9)$$

2. Given a cluster Cl , its centroid is the mean of its members:

$$\text{centroid}_{Eucl}(Cl) = \frac{1}{|Cl|} \sum_{p_i \in Cl} p_i \quad (2.10)$$

3. The distance from point p_i to cluster Cl is the Euclidian distance between p_i and Cl 's centroid:

$$d_{Eucl}(p_i, Cl) = \|p_i - \text{centroid}_{Eucl}(Cl)\| \quad (2.11)$$

Second, in the *ESN-Euclidian* condition, the classical K-means clustered the ESN's responses to the MFCC time series.

1. The set of points $D_{ESN,l}$ contains the earlier collected, unlabeled, ESN responses to the MFCC time series from D_l :

$$D_{ESN,l} = \{X_i | s_i \in D_l\}, \quad (2.12)$$

where X_i is the state collection matrix of the response to MFCC time series s_i .

2. Given a cluster Cl , its centroid is, again, the mean of its members $\text{centroid}_{Eucl}(Cl)$.
3. The distance from point p_i to cluster Cl is, again, the Euclidian distance between p_i and Cl 's centroid $d_{Eucl}(p_i, Cl)$.

Third, in the *ESN-Evidence* condition, conceptors were used as centroids to represent the clusters. In essence, Experiment 1's classifier training procedure provides cluster centroids and its testing procedure acts to reassign points to clusters.

1. The set of points is, again, the ESN responses $D_{ESN,l}$.
2. Given a cluster Cl_j , its centroid is the tuple of the positive conceptor $C_j^{+'}$ and negative conceptor $C_j^{-'}$ computed from its and the other clusters' members:

$$\text{centroid}_{Evid}(Cl_j) = (C_j^{+'}, C_j^{-'}) \quad (2.13)$$

Here, the clusters were construed as a set of classes. The same steps as used to train a phoneme-classifier in Experiment 1 were applied to train a "cluster-classifier". $C_j^{+'}$ and $C_j^{-'}$ are, then, the conceptors representing class i with training instances Cl_j .

3. The distance from point p to cluster Cl_j is the reciprocal of the combined Evidence $E(p, j)$ that p corresponds to cluster class j given the previously trained conceptors in $\text{centroid}_{Evid}(Cl_j)$:

$$d_{Evid}(p, \mu_j) = 1/E(p, j) \quad (2.14)$$

E indicates similarity on the range $(0, \infty)$ [**Can the combined Evidence be 0 in theory?**];

so, d_{Evid} ranges in $(0, 1)$ with larger values indicating a higher degree of dissimilarity between point p and the centroid μ_j of cluster Cl_j .

Fourth, in the *ESN-Hybrid* condition, the *ESN-Euclidian* and *ESN-Evidence* conditions were combined.

1. The set of points is, again, the ESN responses $D_{ESN,l}$.
2. Given a cluster Cl_j , its centroid is two-fold; It includes the mean of the states of the *ESN-Euclidian* condition and the positive and negative conceptors of the *ESN-Evidence* condition:

$$\begin{aligned} \text{centroid}_{Hybrid}(Cl_j) \\ = (\text{centroid}_{Eucl}(Cl_j), \text{centroid}_{Evid}(Cl_j)) \end{aligned} \quad (2.15)$$

3. The distance from point p to cluster Cl_j is the mean of the distances used in the *ESN-Euclidian* and the *ESN-Evidence* conditions:

$$\begin{aligned} d_{Hybrid}(p, Cl_j) \\ = (d_{Eucl}(p, Cl_j) + d_{Evid}(p, Cl_j))/2 \end{aligned} \quad (2.16)$$

$d_{Eucl}(p, Cl_j)$ and $d_{Evid}(p, Cl_j)$ are computed using their respective elements in $\text{centroid}_{Hybrid}(p, Cl_j)$.

With these components as parameters, the clustering algorithm was run for 10 trials in each condition.

Evaluation The resulting clusters were evaluated using one intrinsic measure, the *mean intra-cluster dissimilarity* (MICD), and two extrinsic measures, the *normalized mutual information* (NMI) and *cluster classification accuracy* (CCA).

First, the MICD is the mean dissimilarity between the clusters' centroids and member points across clusters. It is a measure of cluster cohesion ("tightness"), which contributes to clusters being *distinct*. In the interpretation of clusters as symbols (patterns of ESN activity), cluster cohesion translates to a similarity of symbol prototypes to symbol instances. Moreover, it resembles the optimization objectives of the algorithm in the different conditions, and a downward trend of the MICD over the iterations is expected. Thus, it was applied to inform about cluster cohesion and the convergence behavior of the

algorithm. d_{Evid} not being a metric, it also does not fulfill the assumptions of many alternative intrinsic cluster quality measures like the within-cluster sum of squares or the silhouette coefficient. Importantly, the MICD should not be mistaken as a means to compare between conditions, since they used different dissimilarity functions and data types. Given a clustering $Cl = \{Cl_1, Cl_2, \dots, Cl_K\}$, where Cl_k is the set of points assigned to cluster k , the MICD is calculated as follows. For any cluster Cl_k , let the intra-cluster dissimilarity (ICD) be the mean dissimilarity between its member points p_i and its centroid $\text{centroid}(Cl_k)$:

$$ICD(Cl_k) = \frac{1}{|Cl_k|} \sum_{p_i \in Cl_k} d(p_i, \text{centroid}(Cl_k)) \quad (2.17)$$

where $d(p_i, \text{centroid}(Cl_k))$ is the dissimilarity function and depends on the condition. The MICD is then the mean of the ICD values for all clusters:

$$MICD = \frac{1}{K} \sum_{k=1}^K ICD(Cl_k) \quad (2.18)$$

where K is the number of clusters.

Second, the NMI is an extrinsic measure of the similarity between a clustering $Cl = \{Cl_1, Cl_2, \dots, Cl_K\}$, where Cl_k is the set of points assigned to cluster k , and the ground-truth phonemic groups $G = \{G_1, G_2, \dots, G_{|P_l|}\}$, where G_p is the set of points with label p in the dataset D_l . Its values range from 0 for completely dissimilar clusterings and 1 for identical clusterings. It was used to compare the empirically found clusters with the phonemic classes of TIMIT. To compute the NMI, the mutual (shared) information I between Cl and G is normalized by the mean entropy (uncertainty) H within each clustering:

$$\begin{aligned} I(G, Cl) &= \sum_{G_p \in G} \sum_{Cl_k \in Cl} P(G_p \cap Cl_k) \log \frac{P(G_p \cap Cl_k)}{P(G_p)P(Cl_k)} \\ H(G') &= - \sum_{G'_p \in G'} P(G'_p) \log P(G'_p), \text{ for some clustering } G' \\ NMI(G, Cl) &= \frac{I(G, Cl)}{\frac{1}{2}[H(G) + H(Cl)]} \end{aligned} \quad (2.19)$$

Third, I evaluated how accurately the conceptors derived from the clusters could classify new phonemes. This extrinsic measure, that I will refer to as *cluster classification accuracy* (CCA), ought to measure how accurately the acquired symbols this system could be used to represent certain entities, phoneme utterances in this case. Therefore, it was assumed that each cluster corresponded to one of the phonemic classes P . A bijective mapping of clusters to classes was made using Kuhn-Munkres algorithm to maximize the sum of intersections (Plummer and Lovász (1986) mentioned in Song, Liu, Huang, Wang, and Tan (2013)). Then, Experiment 1 was essentially replicated; a conceptor-based classifier was trained on the clusters to classify the respective matched class. The classifier was tested on the phonetically diverse utterances of phonemes P_l that remained from the eight selected speakers.

Run Algorithm 2.2 was repeatedly run on each condition for 20 *trials* to reduce the effects of the random cluster initialization. Thus, 20 replicates \times 20 trials \times 4 conditions = 1600 trials were performed in total. To limit the scope of this study, only a number of $K = 7$ clusters, consistent with the number of phonemic classes $|P_l|$, were searched for.

Results Table 2.3 compares the mean scores of the extrinsic performance measures (columns) of the clustering results across conditions (rows). Two additional rows were added, 'Random clusters' and 'Dataset classes', with the scores to expect of a random clustering and a clustering that perfectly matched the true class labels, respectively. The scores in all conditions were significantly above random [Any way to support the significance claim?]. Between the conditions, *MFCC-Euclidian* outperformed the others in terms of NMI by very little. No significant differences in NMI could be found between the ESN-based conditions. The *ESN-Mixed* condition and the *MFCC-Euclidian* outperformed the others in their accuracy.

Figures 2.3 and 2.4 depict the normalized MICDs and NMIs over the iteration. Horizontal lines provide comparison to the scores of randomly initialized clusters and the "ground truth" scores of the dataset's classes. The MICDs were rescaled to a unit range for all condition, to visualize all of their

Condition	NMI	CCA
MFCC-Euclidian	0.4934	0.5195
ESN-Euclidian	0.4774	0.5073
ESN-Evidences	0.4717	0.5040
ESN-Mixed	0.4757	0.5167
Random clusters	0.0871	0.2438
Dataset classes	1.0000	0.6971

Table 2.3: Mean scores of final clusterings between conditions.

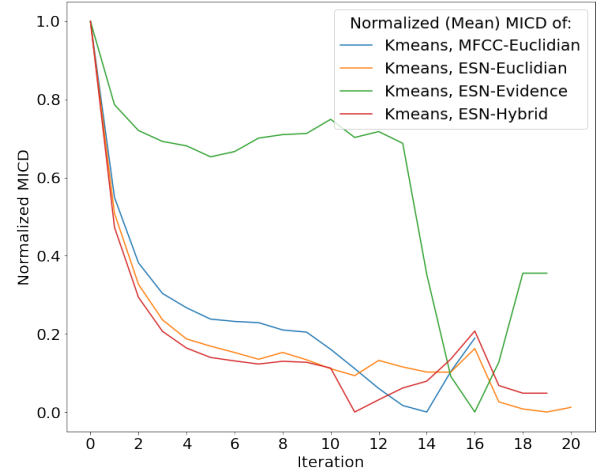


Figure 2.3: The MICDs of the clusterings over the iterations averaged across the trials. [Redo figure replacing "Kmeans" by "Clustering"]

values, initially of different ranges, in one plot. Moreover, the plotted values are the means across trials, excluding any already terminated trials. Since trials terminated at different iterations, the scores at the higher iterations are the means of *fewer* values which explains the increase in variance. For the MICDs, a downward trend exponentially decaying over the iterations can be observed for all conditions. Conversely, the NMIs across conditions increased over the first iteration, after which almost only very slight improvements occurred. Most change in the MICD and NMIs occurred within the first three iterations, with the exception of the .

2.6 Experiment 3: Above-phoneme

The second clustering experiment structures the conceptors C^+ in a hierarchy through an adaptation of HAC. Whereas in Experiment 2, clusters were

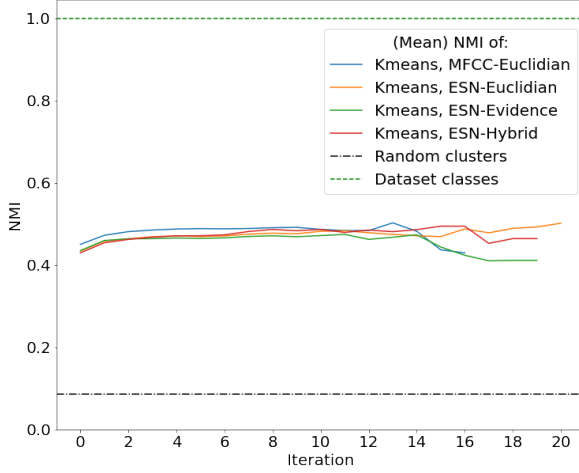


Figure 2.4: The NMIs of the clusterings over the iterations averaged across the trials. For reference, the ideal NMI of clusters corresponding to the dataset’s classes (*Dataset*) and the baseline NMI of randomly initialized clusters (*Random*) are shown as horizontal lines.

identified among ESN states grouped (segmented) by phoneme utterance (more concrete subsymbols), Experiment 3 aims to identify cluster hierarchies among ESN states grouped by phoneme (more abstract subsymbols). The observation that lead to Experiment 3 is that many domains, like Phonetics, are conceptually structured as hierarchies or taxonomies of symbols of increasing abstraction (semantic space). Therefore, this experiment’s purpose is to see if such hierarchical tree structures can be recovered from an ESN’s representation of the domain (representational space). The positive conceptors capture the geometry of the ESN’s representation of phonemes.

Method I will proceed by describing the generalized HAC algorithm, then elaborate on its three parameters and their used arguments (values). HAC is a clustering algorithm aimed at identifying a hierarchy of clusters among the input data. The algorithm works by initializing one cluster per data point and then iteratively merging the two closest clusters until a single cluster or a desired number of clusters is obtained. The result is a hierarchical structure of nested clusters commonly visualized as a dendrogram.

Algorithm 2.3 Generalized HAC

- [1] Set of points $D = \{p_1, p_2, \dots, p_n\}$
- [2] Dissimilarity function $d(p_i, p_j)$
- [3] Linkage function $d_{link}(Cl_i, Cl_j)$

Initialize a cluster for each point: $Cl \leftarrow D$

while number of clusters > 1 **do**

Find the two most similar clusters:

$$Cl_i, Cl_j \leftarrow \arg \min_{Cl_i \neq Cl_j} d_{link}(Cl_i, Cl_j)$$

Update clusters in Cl :

Remove Cl_i and Cl_j

Add $Cl_{merged} = Cl_i \cup Cl_j$

end while

As shown by its pseudocode, the generalized HAC algorithm requires three parameters. These were set as follows to adapt it to the clustering of conceptors:

1. A set of points. These are classically in Euclidian space. Here, the set of points to be clustered consisted of one conceptor embedding per phonemic class of the corresponding samples in the training set. Therefore, the set of positive conceptors from Experiment 1 was reused:

$$D_{HAC} = C^+ = \{C_p^+ | p \in P\} \quad (2.20)$$

2. A dissimilarity measure between two points p_i and p_j . This is classically the Euclidian distance. Here, the reciprocal of the conceptor similarity of p_i and p_j was used:

$$d(p_i, p_j) = 1 - \text{Sim}(p_i, p_j) \quad (2.21)$$

This function fulfils several desirable properties for a dissimilarity measure: It is non-negative, symmetric, and equals 0 for identical inputs.

3. A function that provides the dissimilarity of two clusters. A common choice is the mean pairwise dissimilarity of the points in the two clusters. This variant of HAC is coined average linkage. Concretely, the linkage function $d_{link}(Cl_i, Cl_j)$ between clusters Cl_i and Cl_j is:

$$\begin{aligned} d_{link}(Cl_i, Cl_j) &= \frac{1}{|Cl_i||Cl_j|} \sum_{p_x \in Cl_i, p_y \in Cl_j} d_{HAC}(p_x, p_y) \end{aligned} \quad (2.22)$$

Results The resulting hierarchy is depicted as a dendrogram in Figure 2.5. Each leaf on the left represents a phonemic group. Moving toward the right, phoneme clusters emerge. The dissimilarities between merged child clusters is the abscissa of their link.

Several overlaps can be identified between the HAC phoneme clustering results and phonetic groups depending on the choice of phonetic model. I will compare the clusters with the classes provided by Pfeifer and Balik (2011) and shown in Figure ??, for their model is based on manner of production that seems the variable most correlated to the HAC clusters. Table 2.4 depicts these overlaps with the phonetic groups in the left column and their associated phonemes in the right column. Each group also corresponds to an HAC cluster with the exception of some **bold** phonemes that were moved between sibling clusters. The two primary clusters encompass consonants and vowels with a dissimilarity of about 0.015. Within the upper, consonants, cluster five subgroups can be identified. The red subcluster corresponds to fricatives and affricates (enclosed), both produced with air friction. The green subcluster encompasses plosives (top) and nasals (bottom). However, instead of the manner of production, the place of production may be considered as the group-determining variable. Thus, several other overlaps of the subclusters of consonants with phonetic groups may be found; the *bilabial* stops /p/ and /b/, the *alveolar* stops /t/ and /d/, the *velar* stops /k/ and /g/, and the *alveolar* fricatives /s/ and /z/ were each assigned to exclusive subclusters.

The lower cluster predominantly consists of vowel sounds. No significant correspondence between the sub-clusters of vowels and their pronunciation position or other articulatory features is apparent.

The phonemes in the Mixed group are considered separately, for their articulatory features resemble both vowels and consonants. The group contains the liquids /l/ and /r/ and semivowels /w/ and /y/. These instances all needed to be moved, since no cluster exclusively corresponded to the mixed group. Lastly, the silence /h#/ is considered separately like by Pfeifer and Balik (2011).

In summary, the table displays how the organization of phonemes derived from HAC coincides with traditional phonetic categories. The large resemblance suggests that the HAC algorithm produced relevant and mostly coherent clusters.

Group	Phonemes of Group
Conso- nants	th f sh z s dh v hh
	Affricatives jh ch
	Plosives p b d t g k dx
	Nasals m n ng
Vowels	ow aa oy ah uh er aw ay ey eh ae iy ih uw
	Mixed l r w y
	Silence h#

Table 2.4: Linguistic groups found within the phoneme clusters that resulted from HAC.

References

- David Arthur and Sergei Vassilvitskii. K-means++ the advantages of careful seeding. In *Proceedings of the eighteenth annual ACM-SIAM symposium on Discrete algorithms*, pages 1027–1035, 2007.
- Ilana Bromberg, Qian Qian, Jun Hou, Jinyu Li, Chengyuan Ma, Brett Matthews, Antonio Moreno-Daniel, Jeremy Morris, Sabato Marco Siniscalchi, Yu Tsao, et al. Detection-based asr in the automatic speech attribute transcription project. In *Eighth Annual Conference of the International Speech Communication Association*, 2007.
- William G Chase and Herbert A Simon. Perception in chess. *Cognitive psychology*, 4(1):55–81, 1973.
- Peter I Frazier. A tutorial on bayesian optimization. *arXiv preprint arXiv:1807.02811*, 2018.
- Herbert Jaeger. Controlling recurrent neural networks by conceptors. *arXiv preprint arXiv:1403.3369*, 2014.
- Nikolaus Kriegeskorte and Rogier A Kievit. Representational geometry: integrating cognition, computation, and the brain. *Trends in cognitive sciences*, 17(8):401–412, 2013.

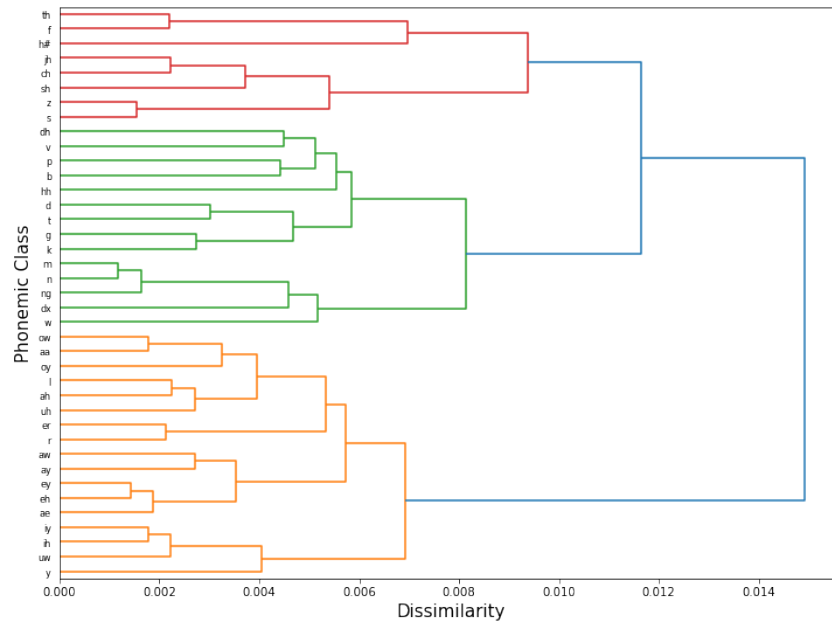


Figure 2.5: Dendrogram of the hierarchy that resulted from the adapted average linkage agglomerative clustering algorithm.

K-F Lee and H-W Hon. Speaker-independent phone recognition using hidden markov models. *IEEE Transactions on Acoustics, Speech, and Signal Processing*, 37(11):1641–1648, 1989.

Lerato Lerato and Thomas Niesler. Investigating parameters for unsupervised clustering of speech segments using timit. In *Twenty-Third Annual Symposium of the Pattern Recognition Association of South Africa*, page 83, 2012.

Mantas Lukoševičius. A practical guide to applying echo state networks. *Neural Networks: Tricks of the Trade: Second Edition*, pages 659–686, 2012.

Brian McFee, Colin Raffel, Dawen Liang, Daniel Ellis, Matt Mcvicar, Eric Battenberg, and Oriol Nieto. librosa: Audio and music signal analysis in python. pages 18–24, 01 2015. doi: 10.25080/Majora-7b98e3ed-003.

George A Miller. The magical number seven, plus or minus two: Some limits on our capacity for processing information. *Psychological review*, 63(2):81, 1956.

Vaclav Pfeifer and Miroslav Balik. Comparison of current frame-based phoneme classifiers. *Ad-*

vances in Electrical and Electronic Engineering, 9, 12 2011. doi: 10.15598/aece.v9i5.545.

Michael D Plummer and László Lovász. *Matching theory*, volume 121. Elsevier, 1986.

Chunfeng Song, Feng Liu, Yongzhen Huang, Liang Wang, and Tieniu Tan. Auto-encoder based data clustering. In *Progress in Pattern Recognition, Image Analysis, Computer Vision, and Applications: 18th Iberoamerican Congress, CIARP 2013, Havana, Cuba, November 20-23, 2013, Proceedings, Part I* 18, pages 117–124. Springer, 2013.

Jamie Vlegels. Multivariate time series classification using conceptors: Exploring methods using astronomical object data. Bachelor’s thesis, University of Groningen, 2022.

A Appendix

A.1 Computing Projector Matrix

The following algorithm for computing projector matrix $P_{R(C) \cap R(B)}$ is taken from Jaeger (2014). C and B are conceptors of size N . We begin by computing the basis matrix $B_{R(C) \cap R(B)}$ as follows:

1. Compute the SVDs
 $C = U \text{diag}(s_1, \dots, s_l, s_{l+1}, \dots, s_N) U'$ and
 $B = V \text{diag}(t_1, \dots, t_m, t_{m+1}, \dots, t_N) V'$, where l and m are the indices of the last singular values if C and B not below the arbitrary threshold $\epsilon_{impr} = 10^{-10} \approx 0$; This approximation [Is this the right word?], but in theory, s_{l+1}, \dots, s_N and t_{m+1}, \dots, t_N should all equal to 0.
2. Let $U_{>l}$ be the submatrix of U made from the last $N - l$ columns of U , and similarly, let $V_{>m}$ consist of the last $N - m$ columns of V .
3. Compute the SVD
 $U_{>l}(U_{>l})' + V_{>m}(V_{>m})' = W \Sigma W'$, where
 $\Sigma = \text{diag}(\sigma_1, \dots, \sigma_k, \sigma_{k+1}, \dots, \sigma_N)$. Again, k is the index of the last singular value of C not below ϵ_{impr} .
4. $B_{R(C) \cap R(B)} = W_{>k}$, the submatrix of W consisting of the last $N - k$ columns of W .

Finally, $P_{R(C) \cap R(B)} = B_{R(C) \cap R(B)} B'_{R(C) \cap R(B)}$.

A.2 Dataset

Table A.1 lists the phone classes and their frequencies within the processed TIMIT dataset.

A.3 Additional Results of Experiment 1

The confusion matrix in Figure A.1 shows the classification rates across the classes.

A.4 Additions of Experiment 2: Hyperparameter Optimization

Hyperparameters $k_b, k_{W^{in}}, r$ and ρ were also tuned automatically using bayesian optimization procedure of the Bayesian Optimization python package. The optimization objective was to maximize

Phone	Folded	#Training	#Test
iy		6953	2710
ih	ix	13693	4654
eh		3853	1440
ae		3997	1407
ah	ax-h ax	6291	2343
uw	ux	2463	750
uh		535	221
aa	ao	6004	2289
ey		2282	806
ay		2390	852
oy		684	263
aw		729	216
ow		2136	777
l	el	6752	2699
r		6539	2525
y		1715	634
w		3140	1239
er	axr	5453	2183
m	em	4027	1573
n	en nx	8762	3112
ng	eng	1368	419
ch		822	259
jh		1209	372
dh		2826	1053
b		2181	886
d		3548	1245
dx		2709	940
g		2017	755
p		2588	957
t		4364	1535
k		4874	1614
z		3773	1273
v		1994	710
f		2216	912
th		751	267
s		7475	2639
sh	zh	2389	870
hh	hv	2111	725
h# (silence)	dcl tcl kcl bcl pcl pau epi q gcl	39467	14021
Σ	39 22	177080	64145

Table A.1: Phone labels and their frequencies. Column 1: Phone classes. Column 2: Phones that were originally present in TIMIT but folded into a class with the left-adjacent phone. Columns 3 & 4: Number of speech samples of each class. Bottom row: Sums of classes or samples.

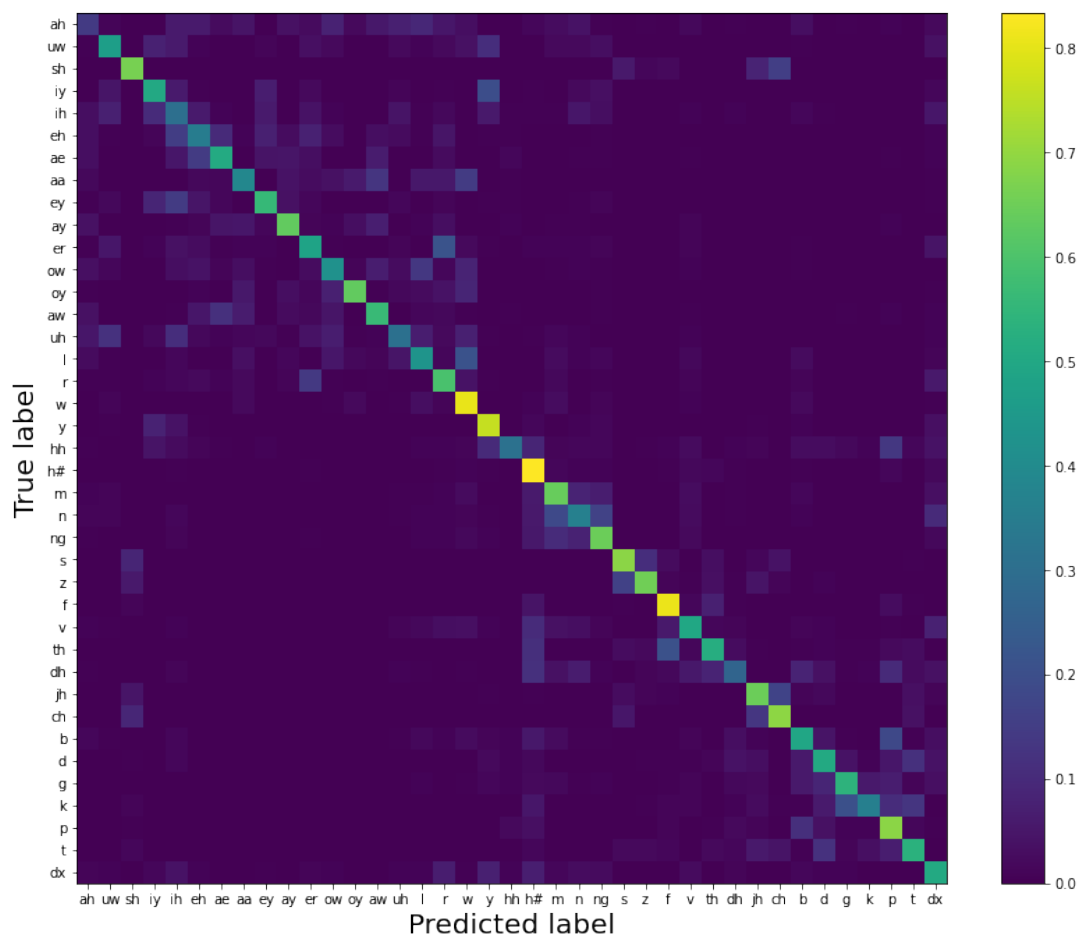


Figure A.1: Multi-class confusion matrix of the classification results. The colors represent the relative frequencies of the predictions (x-axis) made for each of the classes (y-axis). For every phoneme, their rate of correct classification (diagonal entries) was higher than the rate of misclassification to any of other classes (off-diagonal entries) suggesting an above-chance classification accuracy across all phonemic classes. Error rates seem elevated within groups of shared articulatory features like vowels (top left quadrant) and consonants (bottom right quadrant) [Elaborate if necessary].

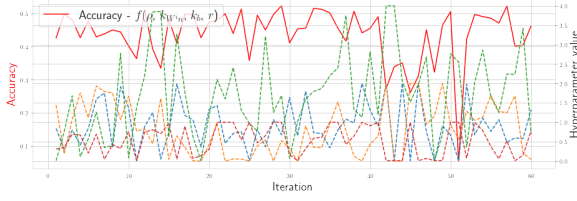


Figure A.2: Hyperparameter tuning with the bayesian optimizer and accuracy [Still no progress seems to occur. This experiment will need to be repeated.]

the testing accuracy of phoneme classification in Experiment 1. Concretely, after 10 initial exploration steps, 40 optimization steps were taken. At each optimization step, a set of hyperparameters is sampled from a promising region of the hyperparameter space trying to maximize an estimated surrogate \bar{f} for the unknown objective function f [$f(\rho, k_{win}, k_b, r) := \text{accuracy}$]. After training and testing the phoneme classifier with these hyperparameters on the training set (with a train-test split), the surrogate estimate is improved (for a detailed review of bayesian optimization, see Frazier). The hyperparameter space was restricted to:

- bias scaling parameter $b \in (0, 2)$
- input weight scaling parameter $k_{win} \in (0.01, 0.99)$
- spectral radius $r \in (0.01, 4)$
- internal weight density $\rho \in (0.01, 1)\%$

The progress of the bayesian optimizer is depicted in Figure A.2. Bayesian optimization was preferred over the more straightforward grid search, since, under consideration of the high computational complexity of training the classifier (about 30 minutes on my computer), the reduced number of training steps outweighed the overhead added by the bayesian optimizer.

A.5 Extension of Experiment 1: Inclusion of input states

Experiment 1 was repeated in slight adaptation of its methods to the stationary type of data. Jaeger (2014) demonstrated that conceptors may be used

to classify signals produced by stationary and non-stationary processes. Stationary processes produce the same kind of signal (with the same probability distribution) over time; for example, white noise or sin waves are the results of stationary processes. Meanwhile, non-stationary processes change their properties over time leading to signals like speech whose probability distributions change over time. Meanwhile in the current classification method, the order within a sequence of states does not affect the resulting conceceptor since it is lost when computing the correlation matrix. This works fine on signals from stationary sources where temporal order is of no relevance. However, for non-stationary sources, states can have different probabilities of occurring depending on their position in the sequence, information not accounted for in the current classification method. Jaeger (2014) approached this limitation by unrolling the ESN response $x(n)_n = 1, \dots, L$ into a vector z reserving a dimension for each step in time. Moreover, the input signal s is appended to z for additional information. We have $z = [x(0); s(0); x(1); s(1); \dots; x(L); s(L)]$. For z , the same classification procedure applies. New hyperparameters were picked by hand; the ESN size was reduced to $N' = 40$ neurons due to the larger computational complexity of this method, but the same density of $r' = 10\%$ was used. Scaling factors were changed to $k'_{win} = 1.5$ and $k'_b = 0.2$. A spectral radius of $\rho' = 1.5$ was used. A training accuracy of 63.64% and test accuracy of 49.13 were reached.

A.6 Additions of Experiment 2

Algorithm A.1 K-means++ improved initialization of centroids.

Require:

Number of clusters K
Set of points $D = \{p_1, p_2, \dots, p_n\}$
Dissimilarity function $d(p_i, p_j)$

Choose first centroid μ_1 uniformly at random from D

for $k = 2$ to K **do**

For each point p_i , compute squared distance to nearest centroid[§]:

$$d_{min}(p_i) = \min_{0 < j < k} d(p_i, \mu_j)^2$$

Choose $p_i \in D$ as the next centroid μ_k with

$$\text{probability } \frac{d_{min}(p_i)}{\sum_{j=1}^n d_{min}(p_j)}$$

end for

return Set of centroids $\mu = \{\mu_1, \mu_2, \dots, \mu_K\}$

B Appendix

B.1 Mathematical notations

Notation	Meaning
A' or x'	Transposes of matrix A or vector x
I	$N \times N$ identity matrix, N to be inferred from context
$[x y]$	Matrix resulting from the column-wise concatenation of vectors x and y
$[x; y]$	Matrix resulting from the row-wise concatenation of vectors x and y
$A[:, y]$	Vector corresponding to the y 'th column of matrix A
$A[x, :]$	Vector corresponding to the x 'th row of matrix A
$ S $	Cardinality of set S
$\ A\ $	Frobenius norm of matrix A
$\text{diag}(A)$	Vector containing the main diagonal of matrix A
$ x $	Magnitude of vector x
A^\dagger	Pseudo-inverse of square matrix A
$R(A)$	Range of matrix A
$\text{tr}(A)$	Trace of square matrix A
P_S	$N \times N$ Projector matrix on the linear subspace S of \mathbb{R}^N , N to be inferred from context
$S \cap Z$	Intersection of linear spaces S and Z

Table B.1: List of some of the mathematical notations used throughout the paper.